Eta Carinae & Other Mysterious Stars
ASP Conference Series, Vol. 242, 2001
T. Gull, S. Johansson & K. Davidson

Raman Scattering and Symbiotic Stars

H. Schmid

Landessternwarte Heidelberg, Königstuhl, D-69117 Heidelberg, Germany

Abstract. Raman scattering by H^0 can occur, if dense neutral regions are strongly irradiated by far-UV radiation. Exactly this condition is meet by symbiotic binaries, where strong far-UV lines from an emission nebula irradiate the neutral gas of a cool giant undergoing heavy mass loss. Therefore, Raman scattering produces different emission features in these systems. In a first part the formation of Raman lines in symbiotic stars is discussed and their spectroscopic properties are summarized.

The second part reviews the diagnostic potential of the Raman scattered O VI lines for symbiotic systems. The measured scattering polarization provides the relative position between light source and scattering region. Therefore, repeated observations reveal the orbital motion of the binary and the inclination and orientation of the orbital plane. This is particularly interesting for systems with extended nebular structures. The diagnostic potential of the O VI Raman lines is further enhanced due to the presence of measurable Doppler shifts introduced by the relative motion of the scatterers enabling the separation of regions with different dynamic velocities. These very favorable properties of the Raman lines provide new information on geometric structures, interaction processes, and mass loss for symbiotic binaries.

1. Introduction

Symbiotic stars are interacting binary systems consisting of a cool giant and a hot radiation source, which is in most cases a white dwarf. The hot component, which typically has a temperature $T_{\rm hot} \approx 100\,000$ K, ionizes parts of the cool giant's wind. This produces a dense and highly ionized nebula, resulting in a strong emission line spectrum. Symbiotic stars form a heterogeneous group of objects. A very useful classification scheme is based on the IR colors: S and D-types (Webster & Allen 1975). The S-types show in the IR normal (stellar) colors of a red giant, while D-types exhibit dust emission. The D-type systems contain often a Mira variable as cool component and have probably very long binary periods $P > 20$ yr. The periods of the more compact S-type systems are about $P \approx 1 - 4$ yr (see Mikolajewska 1997).

The spectra of symbiotic stars often show strong, broad emission bands at λ6825 and λ7082 (Fig. 1). The nature of these features remained for many years unclear until they where identified as Raman scattered O VI lines (Schmid 1989).

The first detection of the stronger emission at λ6825 was reported by Joy & Swings (1945). They observed this line in the recurrent nova RS Oph during the

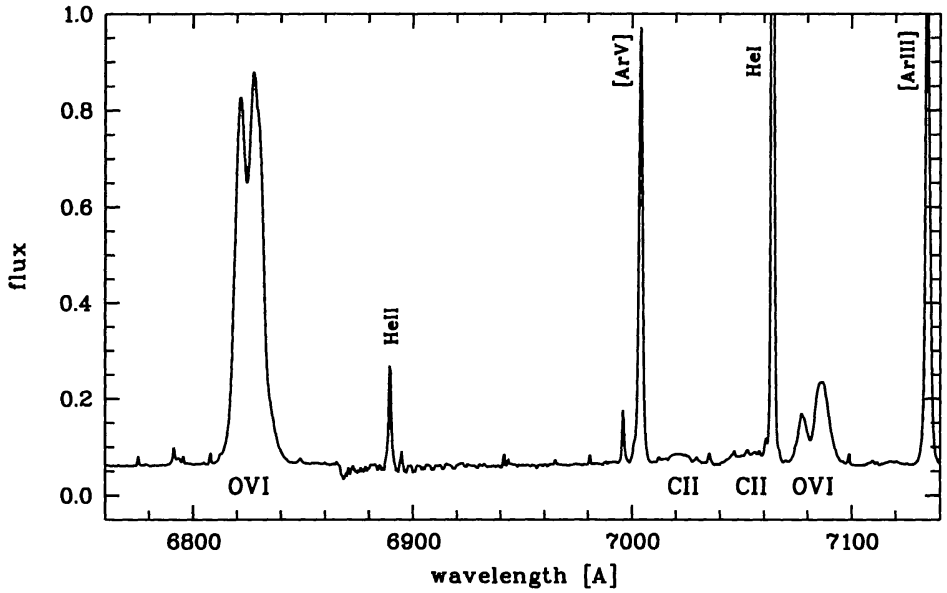

Figure 1. Red spectrum of V1016 Cyg showing the two broad Raman features of O VI at λ6825 and λ7082. In addition the two Raman scattered C II lines at λ7023 and λ7054 are visible as weak, broad bumps. The narrow lines are collisionally excited or recombination lines from the nebula.

1933 outburst, where it was seen together with coronal lines. In later outbursts of RS Oph the λ6825 feature appeared again (e.g. Wallerstein & Garnavich 1986). Allen (1980) found that approximately half of the symbiotic stars exhibit the λ6825 band. In the same paper he extensively discusses their properties and possible identifications. He finds in particular that:

- The λ6825 and λ7082 bands are only observed in symbiotic stars. The intensities of the two features correlate, they show approximately a ratio of $I(\lambda6825)/I(\lambda7082) \approx 4$.
- The band profiles have a typical width of about 20 Å. The profiles vary strongly from star to star but in a given star the two band profiles are similar.
- The λ6825 band is only observed in high excitation systems showing [Ne V] and [Fe VII] lines. Thus the λ6825 emission seems to arise from an ion with an ionization potential above 100 eV.

Raman scattering of the O VI resonance lines $\lambda\lambda$1032,1038 by atomic hydrogen can explain all these properties.

2. Physics and spectroscopy of atomic Raman scattering

2.1. Raman scattering of O VI by H^0

The scattering path of O VI $\lambda\lambda$1032,1038 photons on neutral hydrogen is shown schematically in Fig. 2. The incident photon ν_i excites hydrogen from its ground state $1s\,^2S$ to an intermediate state m from where the Raman-scattered photon ν_f is emitted leaving the atom in the state $2s\,^2S$. The wavelength of the scattered

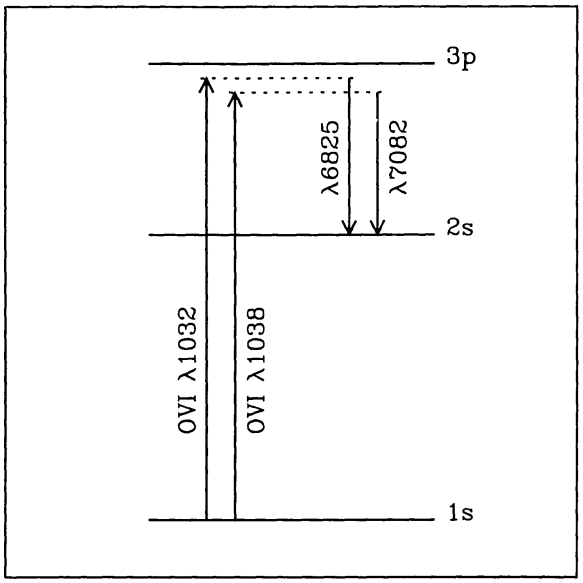

Figure 2. Schematic energy level diagram for Raman scattering of the O VI lines by neutral hydrogen.

photon can be derived on the principle of energy conservation:

$$\nu_f = \nu_i - \nu_{\mathrm{Ly}\alpha}\,, \tag{1}$$

where $\nu_{\mathrm{Ly}\alpha}$ corresponds to the energy difference between the initial and final atomic states.

The scattering cross-section increases rapidly when the intermediate state approaches energetically a bound state (see Fig. 3; Loudon 1983; Sadeghpour & Dalgarno 1992, Lee & Lee 1997a). The O VI doublet lies very close to the H I Lyβ-transition, so that the cross section is large enough $\sigma_{\mathrm{Ram}}(1032) = 7.5\sigma_e$ and $\sigma_{\mathrm{Ram}}(1038) = 2.5\sigma_e$ to produce strong scattering features in symbiotic systems (σ_e: electron scattering cross section).

Raman scattering occurs always together with (elastic: $\nu_f = \nu_i$) Rayleigh scattering. In fact, σ_{Ray} for H^0 is about $3-5$ times larger than σ_{Ram} for the O VI lines. Thus an O VI photon may undergo first one or several Rayleigh scatterings before it is converted into a Raman photon. Rayleigh scattering is often observed in symbiotic systems as enhanced attenuation near Lyα (e.g. Isliker et al. 1989; Vogel 1991; Schmid 1995; Pereira et al. 1999, Dumm et al. 1999). From this it is found that regions of high density H^0 are associated with the cool giant and its surrounding wind region.

The Raman lines are so broad, because a frequency displacement $\Delta\nu$ of the initial O VI photons, e.g. due to the Doppler shift introduced by kinetic or kinematic gas motions, is conserved in the scattering process. Therefore the relative width of the scattered lines $\Delta\nu/\nu_f$ is strongly enhanced compared to the initial line width $\Delta\nu/\nu_i$, in the case of O VI by a factor of about 6.7.

That the Raman scattered O VI lines are only observed in symbiotic systems is not surprising, because it is hard to imagine any other astrophysical configuration, where high density atomic hydrogen gas is so strongly irradiated by O VI photons. In fact, for many symbiotic systems the O VI resonance lines belong to the strongest nebular lines in the entire spectrum (e.g. Espey et al. 1995; Schmid et al. 1999).

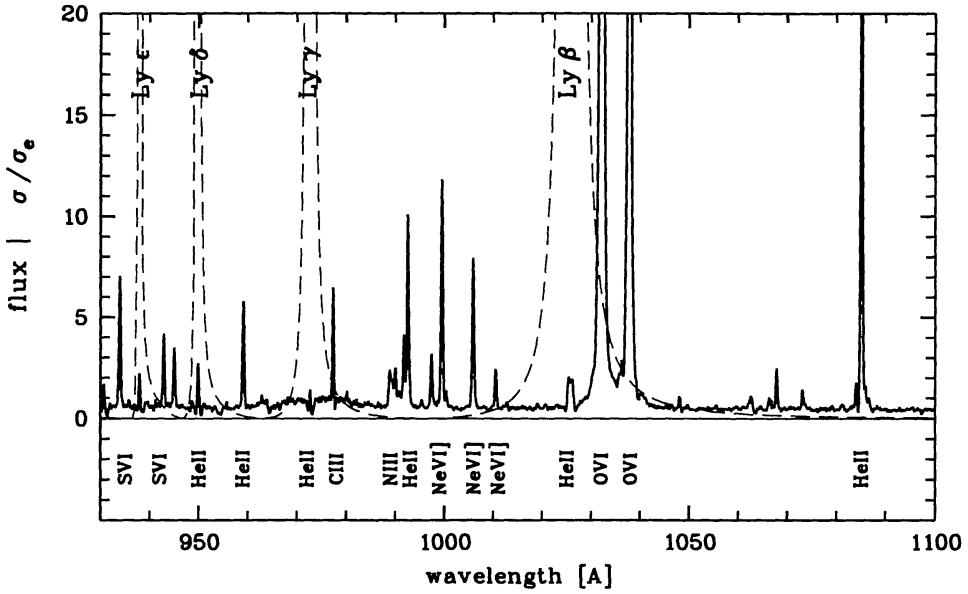

Figure 3. ORFEUS spectrum of RR Tel (Krautter et al. 1998) and Raman scattering cross section in units of σ_e (dashed line, plotted for $\lambda > 937$Å). Strong lines are identified; note that the He II $2-n$ ($n = 4, 6, \ldots$) are very close to the H I Lyman transitions.

2.2. Raman scattering of other far-UV lines by H^0

The λ6825 and λ7082 features in symbiotic systems were the first emission lines in an astronomical object to be identified as the product of a Raman scattering process. However, Raman scattering by neutral hydrogen in not only expected to act on the O VI lines but on all far ultraviolet lines with wavelengths near the H I Lyman transitions (except Lyα) where the scattering cross section is large. It is obvious from Fig. 3 that only a few far-UV emission lines besides O VI have the potential of being Raman scattered by H^0, like the He II $2-n$ ($n = 6, 8, 10\ldots$) transitions or C III λ977.

Indeed, van Groningen (1993) detected weak features of Raman scattered He II $\lambda\lambda$972.1,949.3 at λ4851 and λ4333 in deep spectra of RR Tel. Raman scattered He II λ4851 was also detected in the planetary nebula NGC 7027 (Pequignot et al. 1997).

A weak, double-peaked feature in RR Tel at λ4977 was tentatively attributed to Raman scattered C III λ977 (van Groningen 1993). Unpublished spectra of RR Tel confirm the presence of the double peaked emissions at λ4977. This structure suggests that the C III resonance line profile, as seen by the neutral scattering regions, has a strong central self-absorption.

A further pair of weak broad lines at λ7023 and λ7054 were detected in V1016 Cyg. They can be attributed to Raman scattered C II $\lambda\lambda$1036,1037, (Fig. 1; Schild & Schmid 1996). These features are also visible in deep red spectra of RR Tel. In the far-UV spectrum plotted in Fig. 3 the C II lines are not visible due to circumstellar and interstellar absorption. However, for ionized nebula these lines are expected to be strong.

2.3. Raman scattered line wings for Hα

Most symbiotic systems show Hα lines with broad line wings extending to $\sim$ 500 km/s (e.g. van Winkel et al. 1993). It was proposed by Nussbaumer et al. (1989) that these wings can be formed through Raman scattering of Lyβ photons. For example, if Lyβ is emitted in a broad line region, and subsequently scattered in a cooler or less turbulent environment, then the outer wings of the emission lines fall outside the Doppler profile of the cool region. These photons have therefore a low probability of being converted into Hα via $1s \rightarrow 3p \rightarrow 2s$. However, they may be converted into Hα wing photons by Raman scattering. This mechanism enhances the relative line shift for the Lyβ–Hα wing photons by a factor of $\nu_i/\nu_f = 6.4$. This idea has been strongly supported with a line-fitting analysis on observed profiles of symbiotic stars (Lee 2000) and the planetary nebula IC 4997 (Lee & Hyung 2000).

Thus, Raman scattering must be considered as line broadening mechanism for the strong Balmer transitions in emission line objects with dense H^0-regions.

2.4. Raman scattering by other atoms?

So far we have only discussed Raman scattering by neutral hydrogen. Could also other atoms or ions be responsible for observable Raman scattered lines in astrophysical objects? As the Raman scattering cross sections are small, a potential scattering particle must be abundant and the ratio between the Raman and Rayleigh scattering probabilities must be not too small. The latter point argues against Raman scattering by He^0. But He^+ could be a viable candidate for Raman scattering of EUV-lines near the He II Lyman-series around 230 Å to 260 Å.

Indeed, for the high mass X-ray binary HD 153919 (4U1700–37) an excess emission near He II (2–3) λ1640 was reported by Kaper et al. (1990). This emission appears periodically at phases when the X-ray irradiated hemisphere of the O-star is visible. Kaper et al. (1990) proposed that this could be due to Raman scattering of EUV emission by He^+ in the atmosphere and wind of the extreme O6.5Iaf supergiant. However up to know, it was not possible to associated the observed features with Raman scattered EUV lines. This is also hard, because the EUV spectrum of such systems is unknown. Nonetheless, I consider this currently as most convincing case for atomic Raman lines in an astronomical object not produced by H^0.

For completeness, it is mentioned that Raman scattering by molecular hydrogen H_2 and other molecules is a well known process occurring in planetary atmosphere (see e.g. Betremieux & Yelle 1999 for references).

3. O VI Raman lines as diagnostic tool for symbiotic systems

3.1. Classifications based on the O VI Raman lines

The Raman scattered O VI features are strong lines which are only observed in symbiotic systems. Therefore, they are useful as classification criterion for distinguishing symbiotic systems from planetary nebulae and other objects (e.g. Belczynski et al. 2000).

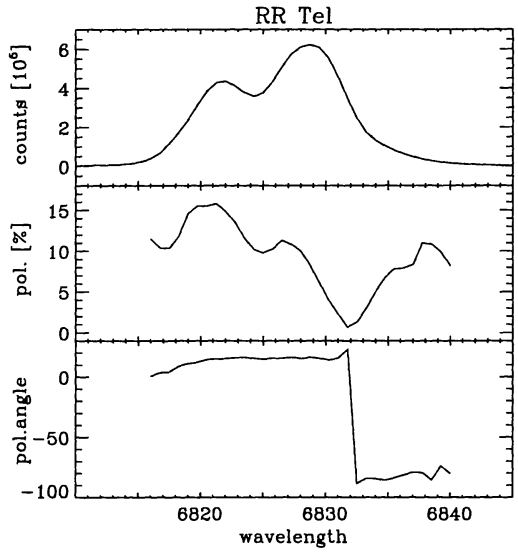

Figure 4. Spectropolarimetric structure of the Raman line λ6825 in RR Tel. The panels give the line photon spectrum (top), the intrinsic percentage polarization (middle) and polarization angle (bottom). The data have been corrected for interstellar polarization and the nebular and stellar continuum has been subtracted (see Espey et al. 1995; Schmid 1996).

The O VI Raman lines are also good indicators for highly ionized emission nebula and for the temperature classification of the ionizing source especially for S-type systems, where the diagnostic nebular lines are strongly suppressed by collisional deexcitation. According to Mürset & Nussbaumer (1994) the presence of the the O VI Raman lines suggests a temperature of $T > 100\,000$ K for the ionizing white dwarf.

3.2. Scattering polarization in the Raman lines

Raman scattering is a dipole type scattering process which produces light polarization, and strong polarization has been detected in the $\lambda\lambda$6825,7082 features (Schmid & Schild 1990). Spectropolarimetric surveys of symbiotic systems show that the Raman lines are practically always polarized. Typically, the integrated line polarization is around $5-10$ %. Most systems show structural variations in the polarization degree and position angle across the line profile. Maximum polarization is usually measured in the blue portion of the line profile, where it can exceed 15%. Further it is found that the polarization structure for a given star is always very similar in both lines (Schmid & Schild 1994; Harries & Howarth 1996b). An example of such spectropolarimetric observations is shown in Fig. 4 for the symbiotic system RR Tel. In RR Tel the two Raman lines consist of a main blue/central polarization component at position angle $\sim 14°$ and a weaker red wing component in each line, separated by a flip of $\sim 90°$ in position angle.

3.3. A simple scattering model

The basic properties of the spectropolarimetric structure in the Raman lines can be explained with a simple scattering model as shown in Fig. 5 (Schmid & Schild 1994). This model is confirmed by detailed Monte Carlo simulations (Schmid 1996; Harries & Howarth 1997; Lee & Lee 1997a,b). The O VI line radiation is produced in a compact region near the hot component. These photons are scattered in the spherically expanding neutral wind of the cool giant. The shape of the H^0–H^+ ionization front depends on the mass loss rate of the cool giant,

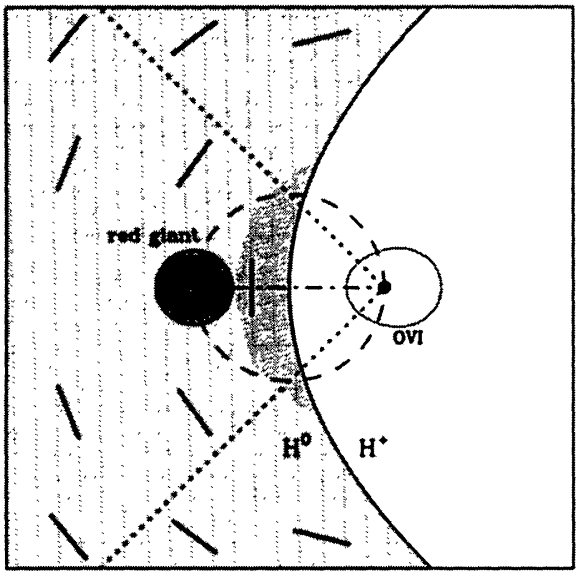

Figure 5. Scattering model geometry for the Raman lines in symbiotic systems. O VI photons originate from near the hot source and are Raman scattered in the neutral wind of the cool giant, mainly in the region facing the hot component (the darker shaded region). The grid of short lines illustrates the induced polarization direction for the scattered Raman photons (see text for more details).

on the ionizing radiation from the hot star and on other interaction processes. The efficiency for producing Raman photons is high for very extended scattering regions (as in Fig. 5) and low if Raman scatterings occur only in and near the cool giant's hemisphere facing the hot component.

The polarization produced in the scatterings is perpendicular to the direction of the incoming photons. The grid of short lines in Fig. 5 shows the resulting polarization angles at different locations.

For a distant observer, who cannot resolve the scattering geometry, the slanted (or the Stokes U) polarization components cancel because of the mirror symmetry of the system. There remain two different scattering regions separated by the diagonal dotted lines (Fig. 5). The quadrant to the left, which includes the cool component, produces a component with a polarization perpendicular to the binary axis, while the sum of the upper and lower quadrants give a parallel component. The resulting net polarization of the total system depends on the relative strength of the contributions from these two regions. For extended scattering region it may result only a small integrated line polarization due to this geometric compensation effect. If the neutral scattering region is confined to a cone around the cool component then we expect a strong polarization ($p > 10\%$) in the Raman line perpendicular to the binary axis.

We can also distinguish two regions if we consider the systematic Doppler shifts introduced in the scattering process. For a spherically expanding neutral wind from the red giant the H^0-atoms inside the dashed circle move towards the O VI source and produce a systematic blue shift in the Raman scattering process. The particles outside this circle move away and produce a red shift in the scattering process.

Putting now the different ingredients together, the following interpretation for the observed Raman line polarization structures can be put forward:

- The polarization in the blue line wings originates in that part of the wind and outer atmosphere of the cool giant which faces and moves towards the hot component.

- A red polarization component originates in the outer part of the giant's wind which moves away from the O VI source.
- A polarization angle flip or rotation is expected if Raman scatterings occur in a very extended region. For systems with a mirror symmetry the polarization angle flip will be 90°.

These properties are mainly due to Raman photons which are produced in the first scattering process. Raman photons produced after one or several Rayleigh scatterings tend to dilute the strong polarization in the O VI lines and smear out systematic Doppler shifts. According to model simulations roughly half of the Raman photons are created after multiple scatterings while the other half are directly scattered (e.g. Schmid 1996).

It is emphasized that many symbiotic systems show a polarization structure in the Raman lines with more than only two position angles. Thus, these systems have no mirror symmetry, and the simple model outlined above can only be a rough approximation (see Sect. 3.5). Further, anisotropic O VI emission due to radiative transfer effects is not considered. This effect may play an important role for the resulting spectropolarimetric structure of the Raman lines (Schmid et al. 1999).

3.4. Polarimetric orbits

The Raman scattering geometry in symbiotic systems rotates relative to the line of sight due to the binary motion. Therefore systematic changes are expected in the polarization signal of the Raman scattered lines which are indeed observed (see references in Table 1).

The determination of orbital parameters from phase locked polarization changes is a well known tool in binary star research (e.g. Rudy & Kemp 1978; Brown et al. 1978). Therefore only a brief description of the principle is given here. For an inclined orbit we expect a polarization minimum at conjunctions. Then the binary configuration is closest to a forward or backward scattering situation which produces no or only little net polarization. The highest polarization will occur at quadratures when the binary configuration is optimal for right angle scatterings. The projection of an inclined circular orbit on the celestial sphere has also an effect on the observed rotation rate in the polarization angle. The angle rotation is relatively fast near conjunction and slow near quadrature. Orbits with small inclinations are always near a right angle scattering configuration. They will show a high percentage polarization with little amplitude together with a steady rotation of the polarization angle.

Thus, phase locked polarization changes can be used to determine the orbit inclination and the orientation of the orbital plane, which are binary parameters often difficult to derive with other methods. Of course, also orbital periods can be derived if not known from other measurements.

S-type systems. Multi-epoch measurements of the Raman line polarization have been reported for 8 S-type systems so far (Table 1). For all systems with known spectroscopic orbits it was found that the Raman line polarization is locked to the orbital motion. Thus, the basic assumptions of the simple scattering model of Sect. 3.3, namely that the O VI emission and the H^0 scattering regions are roughly aligned with the binary axis and closely associated with the stellar hot and cool components are strongly confirmed by these observations. There may

Table 1. S-type symbiotic systems with orbital parameters based on the Raman lines polarization. P_{spec} is the spectroscopic period, p_{max} and p_{min} are the maximum and minimum polarization measured at different epochs, i is the derived inclination, and P_{pol} the period determined from the polarization data (if P_{spec} not known). The objects are ordered according to i and put into two groups with $i > 70°$ and $i < 70°$.

object	P_{spec} [d]	eclipse	p_{max} [%]	p_{min} [%]	i [°]	P_{pol} [d]	Ref
V1329 Cyg	956	yes	13.1	0.2	86		SS1
V445 Sco		?	14.1	0.4	86	1425	HH2
M1-21		?	10.6	1.0	84	892	HH2
SY Mus	624	yes	11.5	1.6	79		HH1,HH2
AG Dra	554	no	4.7	1.9	60		SS2
CD−43°14304	1448	?	7.8	2.2	58		HH2
Z And	759	no	9.9	6.1	47		SS3
Hen 1242		?	4.8	1.8	45	1347	HH2

HH1: Harries & Howarth 1996a; HH2: Harries & Howarth 2000; SS1: Schild & Schmid 1997; SS2: Schmid & Schild 1997a; SS3: Schmid & Schild 1997b.

exist small misalignments and temporal variations of the scattering geometry with respect to the binary axis in at least some object. However, this can be considered as second order effect (e.g. Schmid & Schild 1997a).

For three systems (V445 Sco, M1-21, Hen 1242) with no previous orbit information, the binary period was determined from polarization data.

The derived inclinations i are supported by the fact that both known eclipsing systems V1329 Cyg and SY Mus have $i > 70°$ and the known non-eclipsing systems AG Dra and Z And have $i < 70°$. This also strongly suggests that V445 Sco and M1-21 are eclipsing systems as well.

The maximum and minimum polarization p_{max} and p_{min} measured at different epochs is listed in Table 1 for each object. p_{max} and p_{min} refer to the blue portion of the Raman line λ6825. As expected the high inclination systems show larger variations in p than low inclination systems.

Of interest is, that the high inclination systems reach a higher polarization p_{max} around quadrature than low inclination systems. No such systematic difference is expected if the scattering geometry in symbiotic systems is axis-symmetric. This indicates that the scattering geometry observed from a polar direction suffers more geometric compensation of the polarization signal than for edge-on views. A straightforward interpretation is that the neutral scattering region is more extended in the orbital plane than in polar directions. Such a flattened distribution of neutral gas along the orbital plane is also found in the eclipsing system V1329 Cyg from the residual polarization observed during conjunction phases (Schild & Schmid 1997).

Periods for D-type systems. Orbital periods for D-type systems are not known yet. Due to the mere size of the Mira star in these systems it is thought that the binary periods are at least 20 years and probably much longer (Whitelock

Table 2. Variation with time of the integrated line polarization p (in [%]) and θ (in [°]) of the λ6825 line for the symbiotic Miras V1016 Cyg and AS 210. The averaged rotation rate $d\theta/dt$ for the position angle are given at the bottom.

V1016 Cyg				AS 210			
date	p	θ	obs.[a]	date	p	θ	obs.[a]
1991-9-18	1.3	+6	SS96	1993-5-28	4.4	+24	WHT
1992-9-27	1.5	−4	SS96	1993-8-22	4.9	+23	WHT
1993-5-28	1.9	−7	SS96	1995-2-08	4.5	+30	AAT
1994-9-19	2.1	−13	SS96	1997-6-25	3.1	+34	WHT
1997-6-26	3.2	−13	WHT	1998-6-30	3.3	+37	WHT
1998-7-01	2.7	−19	WHT				
$d\theta/dt = -3.6°/\mathrm{yr}$				$d\theta/dt = +2.5°/\mathrm{yr}$			

a: SS96: taken from Schild & Schmid (1996). All other values are preliminary but include a correction for the interstellar polarization. WHT and AAT stand for observations taken at the William Herschel Telescope and the Anglo-Australian Telescope, respectively.

1987). It seems that the Raman line polarization will provide orbital periods for these systems in future.

Repeated observations of the D-type systems V1016 Cyg and AS 210 show a steady rotation in the flux weighted mean polarization angle of the Raman line λ6825 (Table 2). The average rotation rate gives a preliminary estimate on the orbital period of roughly 100 – 150 years. This estimate should be considered very cautiously, because it is an extreme extrapolation based on measurements taken during a minor fraction of the orbit without knowledge on orbital phase, inclination and eccentricity. But future measurements will extend the time base, improve the periods for V1016 Cyg and AS 210, and provide also measurable polarization changes in other D-type systems.

3.5. On the geometric structure of symbiotic systems

Polar or equatorial outflow? The orbit orientation as derived from the polarimetric orbits is very useful for systems with extended nebular structures in order to distinguish between polar or equatorial outflows.

V1329 Cyg is the only S-type object in Table 1 for which an extended nebulosity has been observed (Schild & Schmid 1997). According to an [O III]-filter image taken with HST the nebulosity consists of a $\sim 0.4''$-long, linear structure with a roughly North-South orientation and a smaller extension stretching East-Southeast. Thereby, the main body of the nebulosity is aligned with the orbital plane as derived from the polarimetric orbit. This suggests that the outflow of material occurs preferentially through the equatorial plane.

Extended nebulosities for D-type systems with Raman lines are observed around V1016 Cyg and HM Sge. For these systems, we know only the current orientation of the binary axis from the Raman line polarization. For both systems the orientation of the binary axis is parallel or perpendicular to distinct features in the surrounding nebulosity (Schild & Schmid 1996; Schmid et al. 2000). This indicates that the orientation of the binary axis is of prime importance for the understanding of the nebular structures.

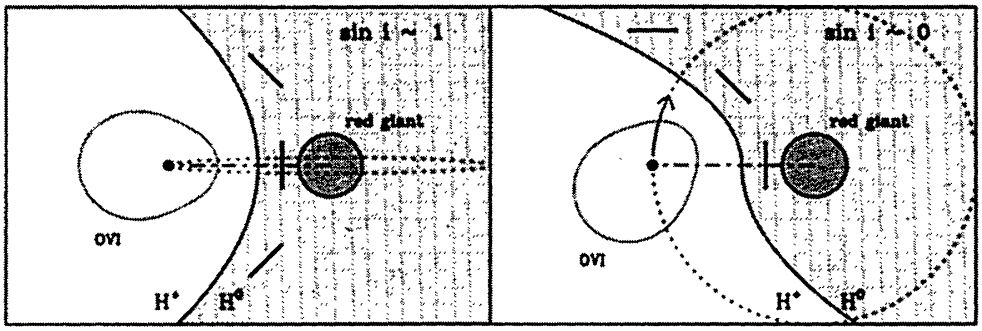

Figure 6. Sketch for the O VI scattering geometry of symbiotic systems viewed "edge-on" (left) and "pole-on" (right). "Edge-on" ($i = 90°$) systems have a mirror symmetry relative to the orbital plane and only polarizations parallel or perpendicular to the binary axis result. In "pole-on" systems the geometry has due to the orbital motion no mirror symmetry. It results a polarization signal with a wavelength (Doppler shift) dependent rotation of the position angles from 0° to 90°.

Raman line profiles and the scattering geometry. As discussed for the simple model in Sect. 3.3, a scattering geometry with an axis-symmetry produces only perpendicular and parallel polarizations. However, many systems show a polarization structure in the Raman lines with more than only two position angles. For these objects we have to abandon rotational symmetry, because such models have a mirror symmetry when projected on the sky.

A tentative model for the 3-dimensional matter distribution, which may explain the polarization profile in the Raman lines of many symbiotic systems, is shown in Fig. 6 (see Schild & Schmid 1996). The model is inspired by hydrodynamical calculations (Walder 1995) which include the effects of orbital motion. It is characterized by a warped ionization front which lags back compared to the "rigid" rotation case. Such a structure still has a mirror symmetry relative to the orbital plane (as in Fig. 6 left). Consequently we should see "symmetric" polarization profiles for systems with inclination close to $i = 90°$. Indeed, the eclipsing systems SY Mus and HBV 475 show a symmetric polarization profile, while non-eclipsing systems, such as Z And, AG Dra have non-symmetric profiles.

Additional investigations are needed to make further progress in our understanding of the geometric structure of symbiotic systems. Thereby, the Raman scattered O VI will play a key role, as their diagnostic potential has only been explored, but has been barely exploited yet. Thus, these lines have a bright future as can be inferred from the past decade where they turned from "just" an unsolved riddle for spectroscopists into perhaps the most important diagnostic lines for symbiotic systems.

Acknowledgments. I am grateful to Hansruedi Schild for many years of fruitful collaboration. This work is supported by a grant from the Deutsche Forschungsgemeinschaft (WO 296/27-1).

References

Allen D.A., 1980, MNRAS, 190, 75
Belczynski K., Mikolajewska J., Munari U., et. al., 2000, A&AS (in press)
Betremieux Y., Yelle R.V., 1999, Icarus 142, 324
Brown J.C., McLean I.S., Emslie A.G., 1978, A&A 68, 415
Dumm T., Schmutz W., Schild H., Nussbaumer H., 1999, A&A 349, 169
Espey B.R., Schulte-Ladbeck R.E., Kriss G.A., et al., 1995, ApJ 454, L61
Harries T.J., Howarth I.D., 1996a, A&A, 310, 235
Harries T.J., Howarth I.D., 1996b, A&AS, 119, 61
Harries T.J., Howarth I.D., 1997, A&AS, 121, 15
Harries T.J., Howarth I.D., 2000, A&A, 361, 139
Isliker H., Nussbaumer H., Vogel M., 1989, A&A, 219, 271
Joy A.H., Swings P., 1945, ApJ 102, 353
Kaper L., Hammerschlag-Hensberge G., Takens R.J., 1990, Nature 347, 652
Krautter J., Appenzeller I., Mandel H., et al., 1998, in: Ultraviolet Astrophysics beyond the IUE Final Archive. ESA, SP-413, p. 347
Lee H.-W., 2000, ApJ 541, L25
Lee H.-W., Hyung S., 2000, ApJ 530, L49
Lee H.-W., Lee K.W., 1997a, MNRAS, 287, 211
Lee K.W., Lee H.-W., 1997b, MNRAS, 292, 573
Loudon R., 1983, The quantum theory of light, Oxford Univ. Press, Oxford
Mikolajewska J. (ed.), 1997, Physical Processes in Symbiotic Stars and Related Systems, Publ. Copernicus Found., Warsaw
Mürset U., Nussbaumer H., 1994, A&A 282, 586
Nussbaumer H., Schmid H.M., Vogel M., 1989, A&A 211, L27
Pequignot D., Baluteau J.P., Morisset C., Boisson C., 1997, A&A, 323, 217
Pereira C.B., Ortega V.G., Monte-Lima I., 1999, A&A 344, 607
Rudy R.J., Kemp J.C., 1978, ApJ, 221, 200
Sadeghpour H.R., Dalgarno A., 1992, J. Phys. B, 25, 4801
Schild H., Schmid H.M., 1996, A&A, 310, 211
Schild H., Schmid H.M., 1997, A&A, 324, 606
Schmid H.M., 1989, A&A, 211, L31
Schmid H.M., 1995, MNRAS, 275, 227
Schmid H.M., 1996, MNRAS, 282, 511
Schmid H.M., Schild H., 1990, A&A, 236, L13
Schmid H.M., Schild H., 1994, A&A, 281, 145
Schmid H.M., Schild H., 1997a, A&A, 321, 791
Schmid H.M., Schild H., 1997b, A&A, 327, 219
Schmid H.M., Krautter J., Appenzeller I., et al., 1999, A&A 348, 950
Schmid H.M., Corradi R., Krautter J., Schild H., 2000, A&A, 355, 261
van Groningen E., 1993, MNRAS 264, 975
van Winkel H., Duerbeck H.W., Schwarz H.E., 1993, A&AS 102, 401
Vogel M., 1991, A&A, 249, 173
Walder R., 1995, IAU Symp. 163, p. 420
Wallerstein G., Garnavich P.M., 1986, PASP 98, 875
Webster B.L., Allen D.A., 1975, MNRAS 171, 171
Whitelock P.A., 1987, PASP, 99, 573

Discussion

Davidson: Can any other lines, other than O VI, be Raman-scattered in an observable way in any objects you can think of?

Schmid: Raman-scattering of the HeII 4-n (n=4, 8, 10) lines by HI in systems with a nebulosity should be examined. Further, molecular hydrogen (H2) could produce Raman lines in systems with a cool giant and strong emission lines. Apart from such systems I am a bit pessimistic as the probability for the formation of Raman lines is too low.

Walborn: Why are the Raman-scattered O VI lines in RR Tel double-peaked?

Schmid: We have made a detailed comparison of line profiles of the direct O VI lines in the far-UV and the Raman-scattered lines for RR Tel. This shows that there are line transfer effects in the O VI resonance lines. So the double peak structure can be explained as O VI self-absorption effect seen indirectly via the scattering region.

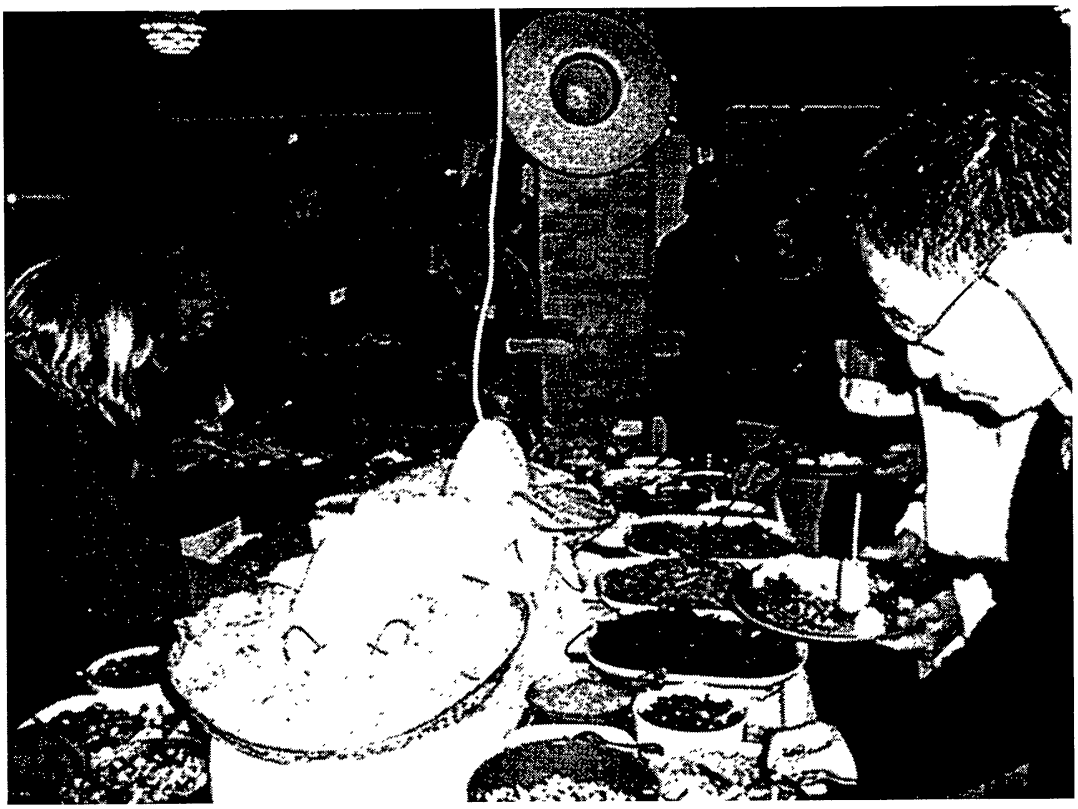

South of the Swedish Border Fiesta